JACS
JOURNAL OF THE AMERICAN CHEMICAL SOCIETY
Article
pubs.acs.org/JACS

Decomposition Products of Phosphine Under Pressure: PH_2 Stable and Superconducting?

Andrew Shamp,[#] Tyson Terpstra,[#] Tiange Bi, Zackary Falls, Patrick Avery, and Eva Zurek*

Department of Chemistry, State University of New York at Buffalo, Buffalo, New York 14260-3000, United States

Supporting Information

ABSTRACT: Evolutionary algorithms (EAs) coupled with density functional theory (DFT) calculations have been used to predict the most stable hydrides of phosphorus (PH_n, n = 1−6) at 100, 150, and 200 GPa. At these pressures phosphine is unstable with respect to decomposition into the elemental phases, as well as PH_2 and H_2. Three metallic PH_2 phases were found to be dynamically stable and superconducting between 100 and 200 GPa. One of these contains five formula units in the primitive cell and has $C2/m$ symmetry (5FU-$C2/m$). It comprises 1D periodic PH_3−PH−PH_2−PH−PH_3 oligomers. Two structurally related phases consisting of phosphorus atoms that are octahedrally coordinated by four phosphorus atoms in the equatorial positions and two hydrogen atoms in the axial positions ($I4/mmm$ and 2FU-$C2/m$) were the most stable phases between ∼160−200 GPa. Their superconducting critical temperatures (T_c) were computed as 70 and 76 K, respectively, via the Allen-Dynes modified McMillan formula and using a value of 0.1 for the Coulomb pseudopotential, μ^*. Our results suggest that the superconductivity recently observed by Drozdov, Eremets, and Troyan when phosphine was subject to pressures of 207 GPa in a diamond anvil cell may result from these, and other, decomposition products of phosphine.

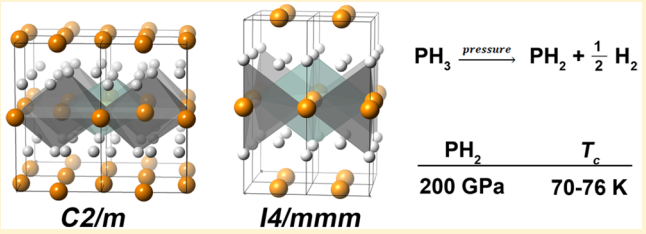

INTRODUCTION

The pressure variable can be used to synthesize materials with unique stoichiometries and properties that would not be accessible otherwise,[1−6] resulting in chemically different bonding motifs that are not observed at ambient conditions.[7,8]

Recent experimental work by Drozdov, Eremets, and Troyan has shown that when hydrides of the p-element sulfur were prepared at $T \geq 300$ K they became superconducting with a critical temperature, T_c, of 203 K at 150 GPa.[9] This work was inspired by first-principles calculations suggesting that at $P >$ 130 GPa H_2S would transform to a phase that has a T_c of 80 K above 160 GPa.[10] The superconducting transition temperatures measured by Drozdov and co-workers for samples prepared at $T \leq 100$ K[9] matched well with the values computed for H_2S.[10] The much higher critical temperature observed experimentally for the sample prepared above room temperature led to the suggestion that the hydrogen sulfide within it decomposed under pressure into a hydride with a stoichiometry that is not stable at 1 atm, and this new phase was responsible for the remarkably high T_c.[9] Indeed, first-principles calculations[11] confirmed that the T_c (computed using the Allen-Dynes modified McMillan equation) of a novel $Im\bar{3}m$-H_3S phase matched exceedingly well with what was observed by Drozdov and co-workers. A plethora of theoretical calculations have verified that the H_3S stoichiometry is indeed the most stable at these pressures, analyzed the factors contributing to T_c, examined anharmonicity as well as the isotope effect, and computed T_c for the related compounds selenium hydride and tellurium hydride.[12−20] A recent combined theoretical and experimental study showed that H_2S can be kinetically protected up to very high pressures and that only H_2S can account for the superconductivity observed in the samples prepared at low temperatures.[19] In addition, a number of other stable decomposition products of hydrogen sulfide, in particular, a superconducting H_4S_3 phase, were identified.[19] These studies highlight that new hydrogen-rich materials can be attained under pressure, some of which may have a T_c higher than values previously thought possible for Bardeen-Cooper-Schrieffer (BCS)-type superconductors,[21] and have invigorated the search for high-temperature superconductivity in high-pressure hydrides. For example, the stability of hydrides with novel stoichiometries containing a group 15 element such as P, As, and Sb have been studied computationally, and the superconducting properties of select systems were examined.[23−25]

Recently, new exciting experiments have revealed that pressure-induced high-temperature superconductivity may be found in other hydrides of a p-block element. Drozdov, Eremets, and Troyan measured superconductivity in phosphine, PH_3, which was liquefied in a diamond anvil cell and subsequently compressed.[22] Resistance measurements revealed a T_c of 30 and 103 K at 83 and 207 GPa, respectively. Structural information on the superconducting phases was not provided. The possible existence of a high temperature superconductor containing phosphorus and hydrogen motivated us to examine

Received: September 28, 2015
Published: January 16, 2016

DOI: 10.1021/jacs.5b10180
J. Am. Chem. Soc. 2016, 138, 1884−1892

the structural landscape of these elements combined under pressure using the evolutionary algorithm XtalOpt. Similar to what was found for H_nS under pressure, it is likely that the observed superconducting properties do not arise from the hydride with the "classic" 1 atm stoichiometry, but instead decomposition products of phosphine, such as PH_2. Between the pressures of 100−200 GPa phosphine is thermodynamically less stable than PH_2 and H_2, and several superconducting PH_2 phases are metastable with respect to solid hydrogen and phosphorus. The T_c computed for the PH_2 structures via the Allen-Dynes modified McMillan equation are significantly larger than those expected for pure phosphorus, approaching the experimental values measured in "phosphine". Our findings therefore suggest that PH_2 may be another hydrogen-rich BCS-type superconductor.

COMPUTATIONAL DETAILS

A priori crystal structure prediction calculations were carried out using the open-source evolutionary algorithm (EA) XtalOpt release 8 and 9[26,27] that has previously been used to predict the structures of a variety of binary hydrogen-rich phases under pressure.[28−32] EA runs were carried out on the PH_3 stoichiometry at 100, 150, and 200 GPa employing simulation cells with 1−6 formula units (FU) at 100 GPa and 2−3 FU at 150 and 200 GPa. In addition, structure searches were performed on the PH_n, n = (1, 2, 4−6), systems at 100, 150, and 200 GPa using cells with 2−3 formula units, unless otherwise noted in Tables S1−S6 in the Supporting Information (SI). Duplicate structures were detected via the XtalComp[33] algorithm. The lowest enthalpy structures from each search were relaxed in a pressure range from 100 to 200 GPa.

Geometry optimizations and electronic structure calculations were performed by using density functional theory as implemented in the Vienna Ab-Initio Simulation Package (VASP) versions 5.2 and 5.4.1,[34] with the gradient-corrected exchange and correlation functional of Perdew−Burke−Ernzerhof (PBE).[35] The projector augmented wave (PAW) method[36] was used to treat the core states, and a plane-wave basis set with an energy cutoff of 700 eV was employed. The H 1s and P 3s/3p electrons were treated explicitly in all of the calculations, using the PAW−PBE H and PAW−PBE P POTCARS available in the potpaw-PBE.52.tar.gz file from the VASP repository. The *k*-point grids were generated using the Γ-centered Monkhorst−Pack scheme, and the number of divisions along each reciprocal lattice vector was chosen such that the product of this number with the real lattice constant was 30 Å in the structure searches, and 40−50 Å otherwise. The *k*-meshes and energy cutoffs used resulted in enthalpies that were converged to within 1 meV/atom. It is likely important to employ density functionals approximating the effects of van der Waals (vdW) interactions for molecular solids containing *p*-block elements near ambient pressure. However, it has been shown that at higher pressures the effect of vdW interactions for these types of systems becomes negligible. For example, by ∼40 GPa dispersion forces were expected to have a minimal effect on the structural parameters, and as a result the properties, of CO_2.[37] For this reason we expect the effect of vdW interactions on the results presented herein, which were obtained between 100 and 200 GPa, to be small. The Nudged Elastic Band (NEB) method[38] was used to construct a reaction pathway between the *I*4/*mmm* and *C*2/*m* PH_2 phases at 200 GPa.

Phonon calculations were performed using the Quantum Espresso (QE)[39] program to obtain the dynamical matrix and electron−phonon coupling (EPC) parameters. In the QE calculations, the H and P pseudopotentials, obtained from the QE pseudopotential library, were generated by the method of Trouiller-Martins with $1s^2$ and $3s^23p^3$ valence configurations, respectively, along with the PBE generalized gradient approximation. Plane-wave basis set cutoff energies were set to 80 Ry for all systems. The Brillouin-zone sampling scheme of Methfessel-Paxton using a smearing of 0.02 Ry and 22 × 22 × 22 *k*-point grids were used for all 100 GPa calculations of the PH_2 2FU-*C*2/*m* and *I*4/*mmm* structures. At 150 and 200 GPa we used *k*-point grids of 24 × 24 × 24 and 30 × 30 × 30 for the PH_2 2FU-*C*2/*m* and *I*4/*mmm* structures, respectively. For the PH_2 5FU-*C*2/*m* structure a 12 × 12 × 12 *k*-point grid was used. Density functional perturbation theory as implemented in QE was employed for the phonon calculations. The EPC matrix elements were calculated using 2 × 2 × 2 *q*-meshes for all of the structures at 100 GPa, as well as for PH_2 5FU-*C*2/*m* at 150 GPa, and the phosphorus structures at all pressures. At 150 and 200 GPa 4 × 4 × 4 and 5 × 5 × 5 *q*-meshes were used for the PH_2 2FU-*C*2/*m* and *I*4/*mmm* structures, respectively. The EPC parameter, λ, was calculated using a set of Gaussian broadenings in steps of 0.005 Ry from 0 to 0.300 Ry. The broadening for which λ was converged to within 0.05 was between 0.015 and 0.040 Ry for all structures. The critical superconducting temperature, T_c, has been estimated using the Allen-Dynes modified McMillan equation[40] as

$$T_c = \frac{\omega_{\log}}{1.2} \exp\left[-\frac{1.04(1+\lambda)}{\lambda - \mu^*(1+0.62\lambda)}\right] \quad (1)$$

where $\omega_{\log}$ is the logarithmic average frequency and μ^* is the renormalized Coulomb potential, often assumed to be between 0.1 and 0.2.

RESULTS AND DISCUSSION

PH_n: Pressure Induced Decomposition of PH_3. Because the phases that PH_3 adopts under pressure are unknown, we have carried out evolutionary searches to predict the global minima configurations up to 200 GPa. A detailed analysis will be published elsewhere, but the coordinates for the most stable structures found at $P \geq 100$ GPa are provided in the SI. Briefly, the 100 GPa phase is made up of layers of PH and hydrogen, whereas the 150 and 200 GPa structures consist of one-dimensional (1D) PH_3−PH_3 networks that resemble those present in the most stable PH_2 structure at 100 GPa discussed below. The computed enthalpies of formation, ΔH_f, of PH_3 with respect to the most stable structures of solid hydrogen[41,42] and phosphorus[43−47] showed that the classic 1 atm stoichiometry is not thermodynamically stable at the pressures considered herein, and potentially even at lower pressures. The ΔH_f for the reaction $\frac{3}{2}H_2(s) + P(s) \rightarrow PH_3$ were computed to be 58.0, 45.2, and 42.6 meV/atom at 100, 150, and 200 GPa, respectively, as illustrated in Figure 1a. In fact, within the 100−200 GPa pressure range all of the hydrides of phosphorus considered herein are thermodynamically unstable with respect to the elemental phases. Our calculations show that at 100 GPa the formation of PH_5 from solid phosphorus and molecular hydrogen would require the least amount of energy, and at 150/200 GPa the stoichiometry with the smallest ΔH_f is PH_2. We find that at 100, 150, and 200 GPa the reaction $PH_3 \rightarrow PH_2 + \frac{1}{2}H_2$ is exothermic, and at 100 and 150 GPa the reaction $PH_3 + H_2 \rightarrow PH_5$ is exothermic. Because the ΔH_f of PH_5 is more positive than that of PH_2 at 200 GPa we focused our analysis on determining if structures with the PH_2 stoichiometry could be metastable (the coordinates for PH_5 are provided in the SI).

Evolutionary searches at 100, 150, and 200 GPa identified three unique low-enthalpy PH_2 phases, whose relative enthalpies are provided in Figure 1b. A *C*2/*m* symmetry system whose primitive cell contained five formula units, 5FU-*C*2/*m*, had the lowest enthalpy excluding zero point energy (ZPE) contributions below 153 GPa. A two formula unit cell with *C*2/*m* symmetry (2FU-*C*2/*m*) and an *I*4/*mmm* structure became preferred at higher pressures. Even though these species are thermodynamically unstable relative to solid phosphorus and H_2 (by at least 38.7, 29.4, and 31.9 meV/

DOI: 10.1021/jacs.5b10180
J. Am. Chem. Soc. 2016, 138, 1884−1892

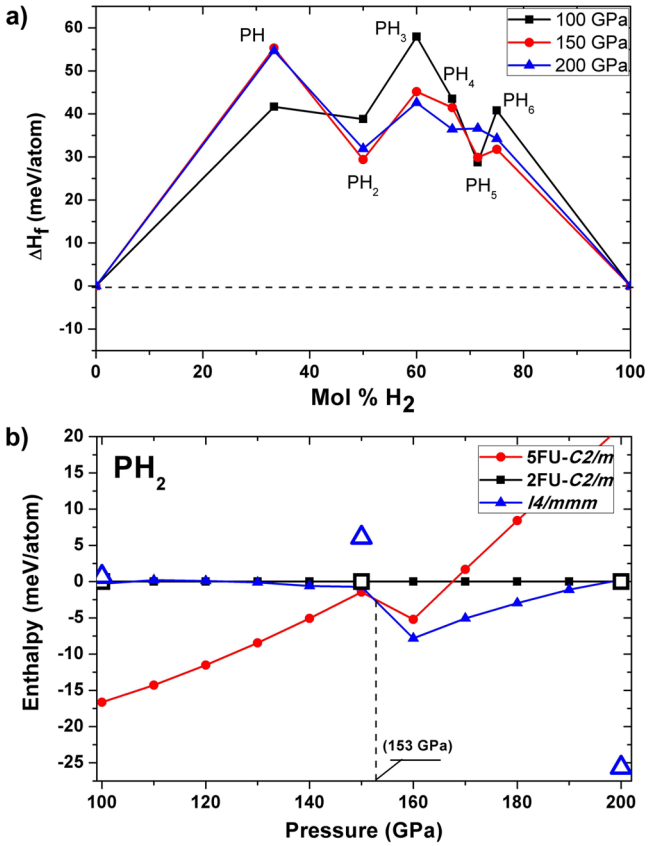

Figure 1. ΔH_f for the reaction $P + \frac{n}{2}H_2 \rightarrow PH_n$ versus the H_2 mole percentage at the pressure range between 100 and 200 GPa. The structural coordinates of the P and H_2 phases used as a reference are provided in the SI. (b) The enthalpies as a function of pressure for the 5FU-*C*2/*m* and *I*4/*mmm* phases of PH_2 relative to 2FU-*C*2/*m* between 100 and 200 GPa. The dashed line indicates the transition pressure below which the 5FU-*C*2/*m* phase has the lowest non-ZPE corrected enthalpy. The open symbols provide the relative enthalpies including the ZPE correction. At 150 GPa the ZPE-corrected enthalpy of 5FU-*C*2/*m* (not shown on the plot) is 45.8 meV/atom higher than that of the 2FU-*C*2/*m* structure.

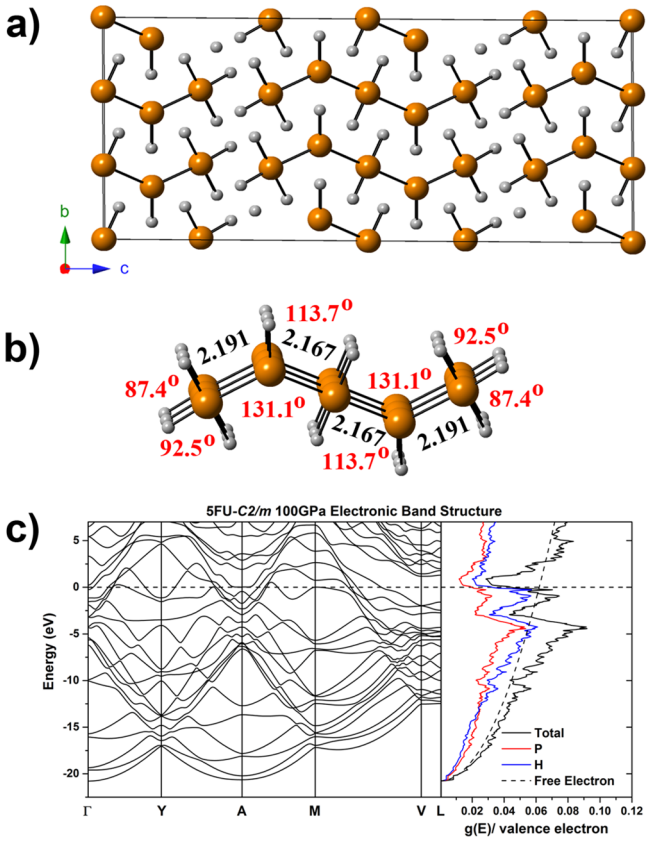

Figure 2. (a) A 3 × 3 × 2 supercell of the 100 GPa 5FU-*C*2/*m* structure. Phosphorus atoms are orange; hydrogen atoms are white. (b) A fragment of the $^1_\infty[PH_3{-}PH{-}PH_2{-}PH{-}PH_3]$ motifs that comprise 5FU-*C*2/*m*. The values provided in black are P−P distances (Å) and the red values are bond angles at 100 GPa. (c) Electronic band structure along with the total and site projected electronic DOS of 5FU-*C*2/*m* at 100 GPa. Because the PDOS for the H and P atoms were relatively independent upon the local atomic environment, we have not decomposed the PDOS into contributions from distinct H and P atoms. E_F is set to zero.

atom at 100, 150, and 200 GPa), they are all dynamically stable within most of the 100−200 GPa pressure range. Moreover, the formation of PH_n with n = 4−6 from PH_2 and H_2 at 100, 150, and 200 GPa, and the decomposition of PH_2 into H_2 and PH at 150 and 200 GPa is computed as being endothermic.

The coordination and arrangement of the phosphorus atoms in 5FU-*C*2/*m* is quite different than in the 2FU-*C*2/*m* and *I*4/*mmm* phases. The former consists of $PH_3{-}PH{-}PH_2{-}PH{-}PH_3$ oligomers extending along the *c*-axis, which are 1D periodic along the *a*-axis, $^1_\infty[PH_3{-}PH{-}PH_2{-}PH{-}PH_3]$ (see Figure 2a,b). The $PH_3{-}PH{-}PH_2{-}PH{-}PH_3$ unit possesses an inversion center of symmetry, with the $H_3P{-}PH$ and $HP{-}PH_2$ distances measuring 2.191 and 2.167 Å, respectively, at 100 GPa. The phosphorus atoms comprising the PH and PH_2 units are coordinated to four other phosphorus atoms forming a square net. Such structural motifs are not uncommon for compressed phosphorus, particularly in the pressure range between 100 and 200 GPa. For example, a number of the high pressure phases of elemental phosphorus, such as the A17 and A7 phases, have been described as Peierls distortions of a simple cubic lattice.[44,48,49] Beyond the A7 phase of black phosphorus, a simple cubic lattice is adopted at ∼11.1 GPa that is stable up to 137 GPa.[43,45,47] After a relatively brief transition through a suspected incommensurate phase,[50,51] simple cubic phosphorus transitions into a simple hexagonal phase[45] followed by a body centered cubic phase adopted at pressures above 262 GPa.[46]

The phosphorus atoms in the $-PH_3$ units at the end of the oligomer are octahedrally coordinated to three hydrogen and three phosphorus atoms, with the H−P−H angles measuring 87.4° and 92.5° and the P−P−P angles measuring 90° at 100 GPa. Similarly, the phosphorus atoms comprising the $-PH_2-$ units at the center of the motif also assume octahedral coordination with four phosphorus atoms on the equatorial and two hydrogen atoms on the axial positions. The phosphorus atoms within the −PH− segment of the oligomer, on the other hand, are nearly trigonal bipyramidal. The axial positions are occupied by two phosphorus atoms, and the equatorial positions are filled by two phosphorus and one hydrogen atom (∠PPP = 131.1°, ∠PPH = 113.7° and 115.2°). At this pressure, all of the P−H distances fall between 1.430 and 1.444 Å, which is close to the typical experimental P−H bond length of 1.437 Å[52] at 1 atm. The P−P distances fall in the range of 2.167−2.191 Å within the oligomer, and measure 2.151 Å

DOI: 10.1021/jacs.5b10180
J. Am. Chem. Soc. 2016, 138, 1884−1892

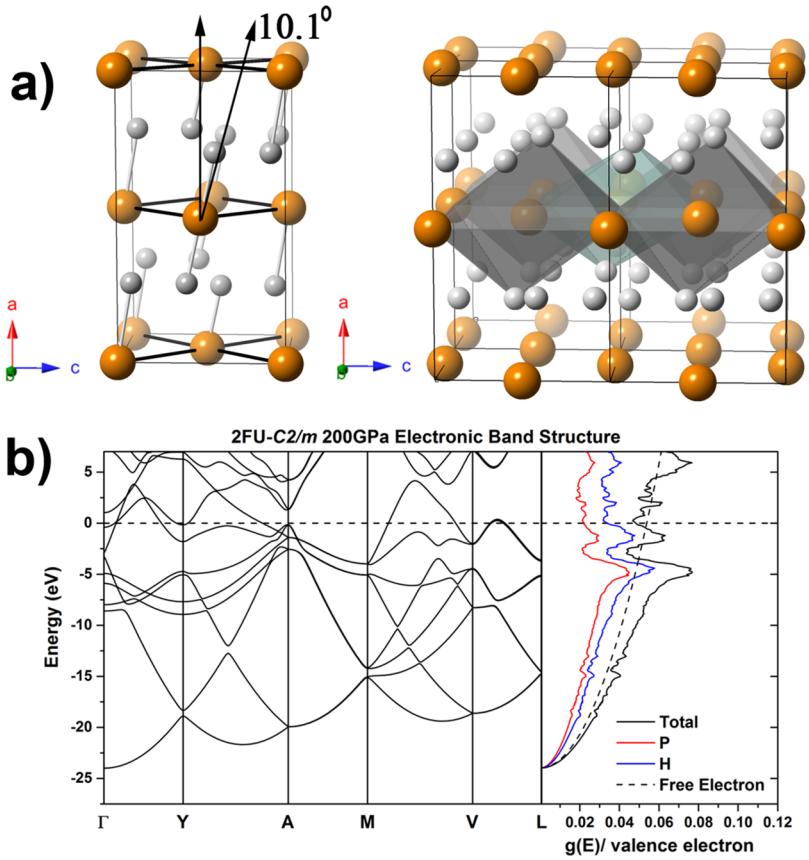

Figure 3. (a) (left) Conventional unit cell and (right) 1 × 2 × 2 supercell of the 200 GPa 2FU-*C*2/*m* phase. Phosphorus atoms are orange; hydrogen atoms are white. (left) The canting angle with respect to a line perpendicular to the plane containing the phosphorus atoms (10.1°) is shown by the arrows. (right) The octahedra around the central plane of phosphorus atoms are highlighted by teal and gray. (b) Electronic band structure along with the total and site projected electronic DOS of 2FU-*C*2/*m* at 200 GPa. E_F is set to zero.

between oligomers, which is comparable to the distance we calculate for elemental phosphorus at this pressure, 2.149 Å.

Figure 2c shows that at 100 GPa 5FU-*C*2/*m*-PH_2 is metallic. The occupied density of states (DOS) is nearly free electron like. But because the Fermi level, E_F, falls near a pseudogap the DOS at E_F, $g(E_F)$ = 0.045 eV^{-1}/valence electron, is lower than the value computed for a free electron gas with the same bandwidth, 0.063 eV^{-1}/valence electron. The metallicity is due primarily to hydrogen states with s-character and also phosphorus states with p-character. The occupied hydrogen and phosphorus states hybridize, indicative of covalent bonding. The electron localization function (ELF), provided in the SI, shows regions of high ELF along the P−P and P−H bonds, and no lone pairs are observed, as would be expected based upon valence-shell electron-pair repulsion (VSEPR) theory, which assumes that the geometry of a molecule minimizes the repulsion between valence shell electron pairs. A Bader analysis revealed electron transfer from phosphorus to hydrogen, with the average charge on the hydrogen atoms being −0.34 at 100 GPa. The charges on the phosphorus atoms in the $-PH_3$, $-PH_2-$, and −PH− units were computed as being +1.12, +0.70, and +0.25, respectively. At 150 GPa the average Bader charges become −0.37 (H), +1.15 (P in $-PH_3$), +0.75 (P in $-PH_2-$), and +0.30 (P in −PH−). Phonon calculations showed that this phase is dynamically stable at 150 GPa.

Above ∼160 GPa two structurally related PH_2 phases, 2FU-*C*2/*m* (Figure 3) and *I*4/*mmm* (Figure 4), become more stable than 5FU-*C*2/*m*. The differences in the enthalpies of these two compounds at 150 and 200 GPa are less than 1 meV/atom, but in between these pressures the non-ZPE corrected enthalpy of the *I*4/*mmm* phase is slightly lower than that of 2FU-*C*2/*m*. The existence of nearly isoenthalpic hydrogen-rich phases under pressure in the DFT calculations is not unprecedented. We have previously found nearly isoenthalpic but distinct structures in our theoretical studies of hydrides containing an alkali metal or alkaline earth metal under pressure. This includes two Li_5H phases that were computed as being more stable than Li and LiH above 50 GPa,[30] five unique CsH_3 structures that were preferred over CsH and H_2 between 30 and 150 GPa,[31] and three BaH_6 phases that had nearly the same enthalpies around 100 GPa.[54]

In both the *C*2/*m* and *I*4/*mmm* phases of PH_2 each phosphorus is octahedrally coordinated by four phosphorus atoms in the equatorial positions and two hydrogen atoms in the axial positions. The difference between the two structures is that, whereas in *I*4/*mmm* all of the atoms assume the ideal octahedral angles, in 2FU-*C*2/*m* the hydrogens are canted with respect to a line that lies normal to the phosphorus square net. At 100 GPa the canting angle is negligible (<0.1°), and the P−P and P−H bond lengths in the two structures are nearly identical (Table 1). At 160 and 200 GPa, however, the canting angle increases to 9.8° and 10.1°, respectively. Even though the nearest neighbor P−P/P−H distances in *I*4/*mmm* are slightly shorter than in 2FU-*C*2/*m* at 160 and 200 GPa, the volume of the former is somewhat larger than that of the latter due to the tilting of the octahedra. The more efficient packing of the

DOI: 10.1021/jacs.5b10180
J. Am. Chem. Soc. 2016, 138, 1884−1892

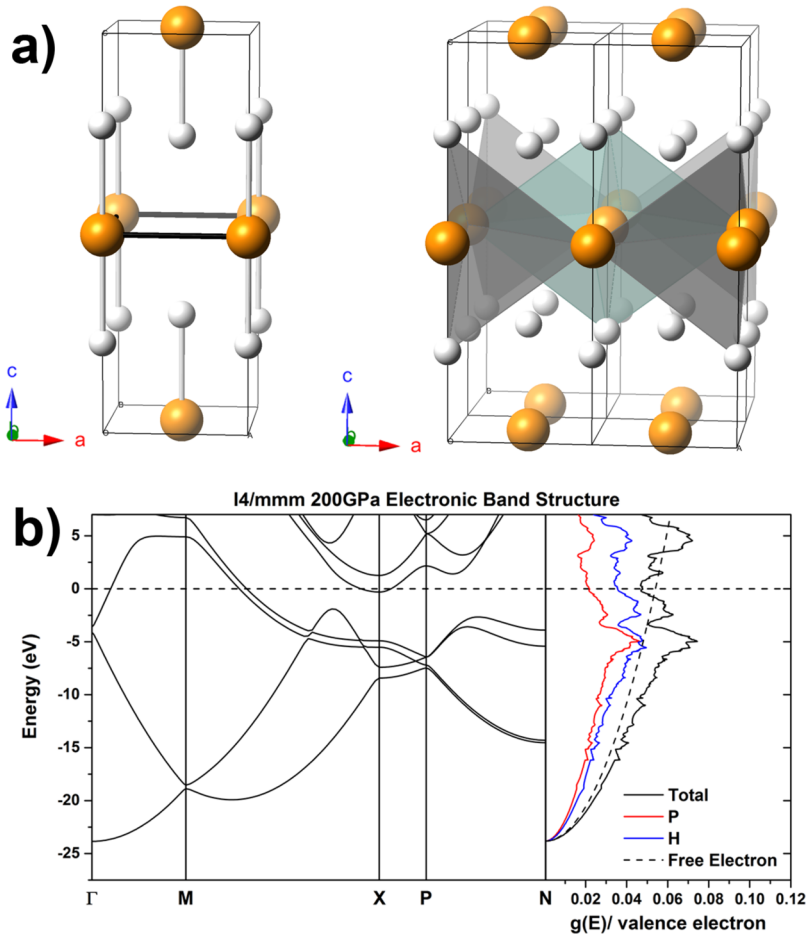

Figure 4. Same as Figure 3 except for $I4/mmm$ PH_2 at 200 GPa. ∠PPP = 90°, ∠HPP = 90°, and ∠HPH = 180°. In the figure on the top right a 2 × 2 × 1 supercell is shown.

Table 1. Phosphorus−Phosphorus, Phosphorus−Hydrogen, and Hydrogen−Hydrogen Distances for the 2FU-$C2/m$ and $I4/mmm$ PH_2 Phases.[a] The Average Bader Charges Per Atom Type are Provided, Along with the Volume Per Unit Cell.

system	pressure (GPa)	P−H(1) (Å)	P−H(2) (Å)	P−P (Å)	H−H(1) (Å)	H (e)	P (e)	volume (Å ^{3}/FU)
2FU-$C2/m$	100	1.449	2.165	2.159	1.527	−0.26	0.53	13.885
	150	1.436	2.013	2.111	1.497	−0.29	0.57	12.398
	160	1.445	1.760	2.127	1.510	−0.27	0.55	12.025
	200	1.439	1.693	2.093	1.500	−0.26	0.52	11.288
I_4/mmm	100	1.449	2.163	2.157	1.528	−0.30	0.60	13.882
	150	1.437	2.012	2.109	1.494	−0.28	0.56	12.401
	160	1.435	1.989	2.101	1.490	−0.28	0.56	12.170
	200	1.434	1.896	2.077	1.487	−0.26	0.52	11.359

[a]P−H(1)/H−H(1) are the first nearest neighbor, and P−H(2) are the second nearest neighbor distances.

octahedra between the layers in the 2FU-$C2/m$ structure, which is a consequence of the canting, can most easily be seen by comparing the P−P distances between the phosphorus atoms comprising different layers. At 100 GPa the separation is identical, 2.983 Å, resulting in comparable volumes. By 160 GPa, however, this distance becomes 2.757 and 2.695 Å for $I4/mmm$ and 2FU-$C2/m$, respectively, giving rise to the sudden difference in volume of 1.2% between the two phases. The PV contribution to the enthalpy is smaller in the more compact 2FU-$C2/m$ phase, but the electronic contribution more strongly favors the more symmetric $I4/mmm$ structure (see the SI), such that $I4/mmm$ is preferred by a few meV/atom for $P \approx 155-195$ GPa. By 200 GPa, however, the two phases become isoenthalpic.

Similar to 5FU-$C2/m$, regions of high ELF in 2FU-$C2/m$ and $I4/mmm$ are found only along the P−P and P−H bonds and the Bader charges in Table 1 are indicative of charge transfer from phosphorus to hydrogen. Both of these phases are good metals with $g(E_F)$ = 0.045−0.048 eV^{-1}/valence electron at 200 GPa, which is close to the value computed for a free electron gas with the same bandwidth, 0.054 eV^{-1}/valence electron. Their DOS plots display many features in common with the DOS calculated for 5FU-$C2/m$: they are indicative of H/P hybridization and the character at the Fermi level is primarily hydrogen s-like, with substantial contributions from phosphorus p-states. Phonon calculations revealed that these two structures are dynamically stable at 100, 150, and 200 GPa.

DOI: 10.1021/jacs.5b10180
J. Am. Chem. Soc. 2016, 138, 1884−1892

Because of the structural similarity between the 2FU-*C*2/*m* and *I*4/*mmm* phases, we wondered if they may be connected via a low energy pathway. The NEB method was employed to find the barrier and transition state between the two structures. The computed barrier was ∼270 meV/atom at 200 GPa, implying that these phases likely lie within two distinct wells on the potential energy surface. The transition state (whose coordinates are given in the SI) can best be described as the average of the two PH_2 phases. Within the NEB method, the positions of the individual atoms within the starting and ending structures must match as closely as possible to avoid large geometric changes that may result in unrealistic barriers. In order to do this the *I*4/*mmm* structure has to be reduced down to its primitive triclinic cell, and then a 2 FU supercell in the crystallographic *b*-direction must be constructed. In the transition state structure the perfect 90° square phosphorus nets described above have been distorted to diamonds with internal angles of 67° and 113° resulting in nearest and second nearest neighbor P−P distances of 1.885 and 2.581 Å (cf. Table 1), and the distance separating the P−P layers is 2.941 Å, which can be compared to 3.017 and 2.963 Å for the *I*4/*mmm* and *C*2/*m* phases, respectively. Each phosphorus is [2 + 4] coordinate to hydrogen. Similar to the two end point structures, the shortest two P−H distances fall between 1.45 and 1.50 Å, which is slightly longer than the distance of a P−H bond in phosphine at ambient conditions, 1.42 Å.[53] The remaining four P−H distances fall within 1.7−1.8 Å, and are different for each phosphorus atom in the P1 symmetry 2FU transition state.

We also wondered if tilting the octahedra to different angles would yield other structures not found in our evolutionary runs whose enthalpies were similar to *I*4/*mmm* and *C*2/*m*. In order to test this hypothesis we relaxed structures constructed to have canting angles of 45°, as well as geometries where hydrogen atoms were placed at random positions within the phosphorus lattice at 200 GPa. No unique low enthalpy structures were found. In addition, a closer inspection of the evolutionary runs showed that structures similar to those we constructed by hand had been generated and optimized during the EA searches, but their enthalpies were significantly higher than 5FU-*C*2/*m*, 2FU-*C*2/*m*, and *I*4/*mmm* PH_2.

Because the ZPE may be large for extended systems containing light elements, we computed the enthalpic differences between these three PH_2 phases including the ZPE corrections at pressures where they were dynamically stable. The open symbols in Figure 1c show that the inclusion of the ZPE makes the *I*4/*mmm* and 2FU-*C*2/*m* structures significantly more stable than 5FU-*C*2/*m* at 150 GPa, with the *C*2/*m* being preferred by 6 meV/atom. Because the 2FU-*C*2/*m* and *I*4/*mmm* phases are structurally similar, their phonon DOS and their ZPE at 150 GPa are nearly identical. The phonon DOS of the 5FU-*C*2/*m* phase, on the other hand, shows that the frequencies associated with the hydrogen vibrations above 2000 cm^{-1} are larger in comparison to these two phases, resulting in a significantly larger ZPE at 150 GPa, which leads to the destabilization of this phase when compared to the other two structures. At 200 GPa the ZPE corrections favor the *I*4/*mmm* phase such that its zero-point corrected enthalpy is 25 meV/atom lower than that of 2FU-*C*2/*m*. The reason for this is that the *C*2/*m* structure has more high frequency modes above 1500 cm^{-1} (see Figure 5). Thus, our results present another example of how the ZPE of phases with light elements can affect their relative enthalpies. It is beyond the scope of this work to consider anharmonic effects to the (free) energies (and

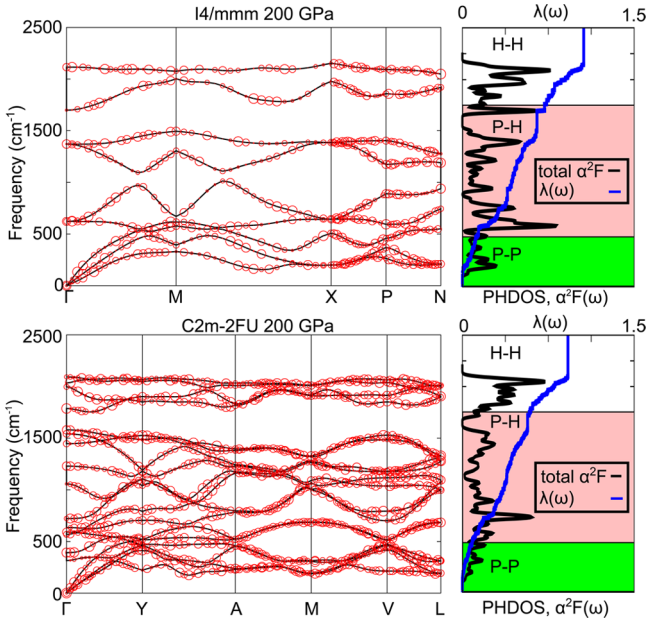

Figure 5. Phonon band structure, Eliashberg spectral function, $\alpha^2F(\omega)$, and the electron−phonon integral, $\lambda(\omega)$, for 2FU-*C*2/*m* and *I*4/*mmm* PH_2 at 200 GPa. Circles indicate the phonon line width with a radius proportional to the strength. The highlighted sections of the $\alpha^2F(\omega)$ plots show the division into vibrational modes that comprise phosphorus vibrations (P−P, green), motions of hydrogen and phosphorus atoms (P−H, pink), and mainly hydrogen vibrations (H−H, white). The contribution toward λ for these divisions are 0.09 (9.3%), 0.50 (54.6%), and 0.33 (36.1%) for 2FU-*C*2/*m* and 0.13 (12.8%), 0.58 (54.9%), and 0.34 (32.3%) for *I*4/*mmm*, for the green, pink, and white divisions, respectively.

T_c), but it may be that these also influence the order of stability of the phases studied herein. To determine if these three PH_2 structures could potentially contribute to the superconductivity observed by Drozdov and co-workers in their compression of phosphine up to 207 GPa, their superconducting properties were investigated in further detail, as described in the following section.

Superconducting Phases of PH_2. Above 5 GPa superconductivity has been observed in black phosphorus, the most stable allotrope at ambient conditions. The experimentally measured T_c depends on the path taken in the pressure/temperature phase diagram. Recent experiments, and DFT calculations using the Allen-Dynes modified McMillan equation, both showed that for the simple cubic phase of phosphorus T_c decreases with increasing pressure.[55,56] Computations revealed that the decrease in T_c above 30 GPa could be explained by the increase in the phonon frequencies, and a μ^* of 0.18 yielded a T_c of 5.8 K at 70 GPa,[56] which agrees well with the experimentally measured T_c of 4.3 K at 100 GPa.[55] At higher pressures, up to 160 GPa, experiments suggested that T_c decreased below 4 K.[55] In comparison, the computational methodology used herein coupled with a μ^* of 0.18 resulted in a T_c of 6.4 K for simple cubic phosphorus at 100 GPa, and slightly higher temperatures for smaller values of the Coulomb pseudopotential (see Table 2). We have also computed the parameters entering the Allen-Dynes modified McMillan equation for simple hexagonal phosphorus at 150 and 200 GPa, so that they may be compared with those calculated for the aforementioned PH_2 phases. As Table 2 shows, the average logarithmic frequency, ω_{log}, of phosphorus

DOI: 10.1021/jacs.5b10180
J. Am. Chem. Soc. 2016, 138, 1884−1892

Table 2. Electron-Phonon Coupling Parameter (λ), Logarithmic Average of Phonon Frequencies (ω_{log}), and Estimated Superconducting Critical Temperature (T_c) for Values of the Coulomb Pseudopotential (μ^*) of 0.1 and 0.18 for Simple Cubic (S.C.) Phosphorous, Simple Hexagonal (S.H.) Phosphorous, and the 5FU-C2/m, 2FU-C2/m, and $I4/mmm$ PH_2 Phases at Various Pressures

system	pressure (GPa)	λ	ω_{log} (K)	$T_c^{\mu^*=0.1}$ (K)	$T_c^{\mu^*=0.18}$ (K)
S.C. P	100	0.66	521.7	15.9	6.4
S.H. P	150	0.21	575.6	0.0	0.0
S.H. P	200	0.13	671.8	0.0	0.0
5FU-C2/m	100	1.05	655.1	49.0	32.1
5FU-C2/m	150	1.00	798.1	55.5	35.2
2FU-C2/m	200	1.04	1026.5	75.6	49.2
$I4/mmm$	150	0.86	946.2	50.6	28.3
$I4/mmm$	200	1.13	851.6	70.4	48.0

increases with pressure and the electron−phonon coupling, λ, decreases, quenching the superconductivity within the simple hexagonal phase.

How would the incorporation of H atoms within the phosphorus lattices, in the most stable PH_2 geometries, affect the ω_{log}, λ, and T_c? To answer this question we computed the superconducting properties of the previously discussed PH_2 phases, at pressures where they were found to be dynamically stable, and the results are given in Table 2. Figure 5 provides the phonon band structure and line widths, Eliashberg spectral function, and plots the dependence of λ on the frequencies for the 2FU-C2/m and $I4/mmm$ phases at 200 GPa (analogous plots can be found in the SI for all of the other T_c values computed herein). In pure compressed hydrogen it has been proposed that μ^* can range from 0.08 to 0.089,[57,58] whereas values of 0.18[56] have been employed for simple cubic phosphorus at 100 GPa. We therefore list critical temperatures computed for μ^* of 0.1 and 0.18 in Table 2. However, because the generally accepted value for the Coulomb pseudopotential is within 0.1 to 0.13, the text quotes T_c values computed for a μ^* of 0.1.

Because of the structural similarities between $C2/m$ and $I4/mmm$ at 150 GPa, their critical temperatures should be nearly identical, and T_c was calculated as being 51 K for the $I4/mmm$ structure. The aforementioned canting of the octahedra results in geometric changes between these two structures at higher pressures, which could potentially affect the superconducting properties. Indeed, at 200 GPa the electron phonon coupling of $I4/mmm$ was calculated as being somewhat larger than for $C2/m$, but ω_{log} was nearly 175 K larger for $C2/m$ because the vibrational modes arising primarily from hydrogen atoms are, on average, found at higher frequencies in this phase. The canting results in a larger number of hydrogen atoms that are found within a distance of 2 Å of a given hydrogen in $C2/m$, thereby increasing the frequencies associated with their vibrations. For example, whereas $I4/mmm$ has four H−H distances at 1.486 Å, in $C2/m$ the H−H measures are 1 × 1.497 Å, 1 × 1.507 Å, 2 × 1.585 Å, and 2 × 1.775 Å. Because of the opposing effects of ω_{log} and λ on the critical temperature, the T_c values computed for the $C2/m$ (76 K) and $I4/mmm$ (70 K) phases at 200 K are very similar despite their structural differences.

At 200 GPa the most significant contribution to λ in the 2FU-C2/m and $I4/mmm$ PH_2 systems stems from vibrational modes between 500 and 1750 cm^{-1} that involve hydrogen and phosphorus motions. The electron phonon coupling arising from modes above 1750 cm^{-1}, which consist primarily of the motion of hydrogen atoms with a small contribution from the phosphorus atoms, are also substantial components of the total λ. Vibrations below 500 cm^{-1}, which are the result of phosphorus motions, play a small but non-negligible role in the electron−phonon coupling. The computed T_c of the PH_2 phases are significantly larger than for monatomic phosphorus because hydrogen increases both ω_{log} and λ. The electron phonon coupling is in line with the values typically computed for compressed hydrogen-rich phases, 0.5−1.6,[59−61] but smaller than the values of 2.19 at 200 GPa and 2.69 at 150 GPa computed for $Im\bar{3}m$ H_3S[11] and CaH_6,[62] respectively. The phonon line widths reveal that unlike CaH_6,[62] where the electron phonon coupling was derived primarily from a single vibrational mode, a plethora of modes contribute toward λ in PH_2.

The superconducting critical temperatures we compute for the $I4/mmm$ and 2FU-C2/m phases of PH_2 are somewhat lower than the experimentally measured value of 103 K at 207 GPa.[22] However, it may be that the T_c measured by Drozdov and co-workers results from a mixture of phases. For example, recent experimental work has suggested that the decomposition of LiH under pressure in a diamond anvil cell may lead to the formation of layers with different LiH_n stoichiometries.[63] This work was inspired by theoretical predictions,[64] and observables computed via DFT calculations were employed to aid the interpretation of the experimental results. Pepin and co-workers suggested that under pressure Li diffuses into the diamond anvil cell forming a LiH_6 layer at the diamond/sample interface, and an LiH_2 layer at the LiH_6/LiH interface. Such mechanisms may also be important for the pressure induced decomposition of phosphine, and it is only via comparison of the computed experimental observables for specific phases with the results obtained experimentally that one can uncover which phases are formed under pressure, and the mechanisms underlying their formation. A feedback loop between experiment and theory is integral to advance our understanding of high pressure phenomena, as recent work on compressed hydrogen sulfide has shown.[19]

The decrease in T_c with pressure of all of the PH_2 phases considered herein correlates with the markedly lower critical temperature, 30 K, measured by Drozdov and co-workers at 83 GPa. In future work we will focus on predicting the structures of PH_n phases at pressures where vdW interactions may be important, and interrogate their bonding and superconducting properties.

CONCLUSIONS

Recent experiments revealed that when PH_3 is compressed to 207 GPa, it becomes superconducting below 103 K.[22] Our density functional theory (DFT) calculations have shown that at pressures of 100, 150, and 200 GPa PH_3 is thermodynamically unstable with respect to decomposition into the elemental phases, as well as PH_2 and H_2. Based upon the computed enthalpies other reactions that may occur under pressure are $PH_3 + H_2 \rightarrow PH_5$ (100 and 150 GPa) and $PH_2 \rightarrow \frac{1}{2}H_2 + PH$ (100 GPa). *A priori* crystal structure prediction has been used to identify three PH_2 phases that are dynamically stable in the pressure range of 100−200 GPa. All of these are calculated to be superconducting via the Allen-Dynes modified McMillan

DOI: 10.1021/jacs.5b10180
J. Am. Chem. Soc. 2016, 138, 1884−1892

equation, suggesting that like H_3S,[9] PH_2 may be another hydrogen-rich Bardeen-Cooper-Schrieffer (BCS)-type superconductor.

Two PH_2 structures with $C2/m$ and $I4/mmm$ symmetry were computed to have a superconducting critical temperature, T_c, of 76 and 70 K, respectively, at 200 GPa. Between 150 and 200 GPa the non-ZPE (zero point energy) corrected enthalpies of these phases differed by only a few meV/atom, and their structures both consisted of square nets of phosphorus atoms. In the $I4/mmm$ structure the phosphorus atoms were octahedrally coordinated, with two hydrogen atoms in the axial positions. In the $C2/m$ phase the hydrogens are slightly canted from the ideal octahedral angles allowing the distance between the planes of phosphorus atoms to decrease, and reducing the volume of the structure. A five formula unit phase with $C2/m$ symmetry (5FU-$C2/m$), which consists of 1-D PH_3−PH−PH_2−PH−PH_3 oligomers, was also identified in our evolutionary searches, and it has the lowest non-ZPE corrected enthalpy at 100 GPa. At this pressure its T_c is computed to be 49 K. Upon decreasing the pressure, the T_c of all of the PH_2 phases decreased.

Our results provide another example of how pressure can lead to the formation of compounds with stoichiometries and properties that would not be predicted based upon our experience at 1 atm. Comparison of the observables computed for these PH_2 phases with results obtained experimentally will unveil which phase, or mixture of phases, give rise to the superconducting properties observed by Drozdov and coworkers.[22]

■ ASSOCIATED CONTENT

Supporting Information

The Supporting Information is available free of charge on the ACS Publications website at DOI: 10.1021/jacs.5b10180.

Details of the structure searches, band structures, structural parameters, electronic and phonon DOS plots, absolute energies in Hartree, phonon convergence plots, and Nudged Elastic Band results (PDF)

■ AUTHOR INFORMATION

Corresponding Author

*E-mail: ezurek@buffalo.edu.

Author Contributions

#Andrew Shamp and Tyson Terpstra contributed equally.

Notes

The authors declare no competing financial interest.

■ ACKNOWLEDGMENTS

We acknowledge the NSF (DMR-1505817) for financial, and the Center for Computational Research (CCR) at SUNY Buffalo for computational support. A.S. acknowledges financial support from the Department of Energy National Nuclear Security Administration under Award Number DE-NA0002006, and E.Z. thanks the Alfred P. Sloan Foundation for a research fellowship (2013-2015). A.S. also acknowledges Daniel P. Miller for his help with using the Nudge Elastic Band Method.

■ REFERENCES

(1) Grochala, W.; Hoffmann, R.; Feng, J.; Ashcroft, N. W. *Angew. Chem., Int. Ed.* **2007**, *46*, 3620−3642.
(2) Zurek, E.; Grochala, W. *Phys. Chem. Chem. Phys.* **2015**, *17*, 2917−2934.
(3) Hermann, A.; Schwerdtfeger, P. *J. Phys. Chem. Lett.* **2014**, *5*, 4336−4342.
(4) Hermann, A.; McSorley, A.; Ashcroft, N. W.; Hoffmann, R. *J. Am. Chem. Soc.* **2012**, *134*, 18606−18618.
(5) Peng, F.; Miao, M.; Wang, H.; Li, Q.; Ma, Y. *J. Am. Chem. Soc.* **2012**, *134*, 18599−18605.
(6) Peng, F.; Yao, Y.; Liu, H.; Ma, Y. *J. Phys. Chem. Lett.* **2015**, *6*, 2363−2366.
(7) Lu, C.; Miao, M.; Ma, Y. *J. Am. Chem. Soc.* **2013**, *135*, 14167−14171.
(8) Yao, Y.; Hoffmann, R. *J. Am. Chem. Soc.* **2011**, *133*, 21002−21009.
(9) Drozdov, A. P.; Eremets, M. I.; Troyan, I. A.; Ksenofontov, V.; Shylin, S. I. *Nature* **2015**, *525*, 73−76.
(10) Li, Y.; Hao, J.; Liu, H.; Li, Y.; Ma, Y. *J. Chem. Phys.* **2014**, *140*, 174712.
(11) Duan, D.; Liu, Y.; Tian, F.; Li, D.; Huang, X.; Zhao, Z.; Yu, H.; Liu, B.; Tian, W.; Cui, T. *Sci. Rep.* **2014**, *4*, 6968.
(12) Flores-Livas, J. A., Sanna, A., Gross, E. K. U. *arXiv:1501.06336v1*.
(13) Papaconstantopoulos, D. A.; Klein, B. M.; Mehl, M. J.; Pickett, W. E. *Phys. Rev. B: Condens. Matter Mater. Phys.* **2015**, *91*, 184511.
(14) Bernstein, N.; Hellberg, C. S.; Johannes, M. D.; Mazin, I. I.; Mehl, M. J. *Phys. Rev. B: Condens. Matter Mater. Phys.* **2015**, *91*, 060511.
(15) Duan, D.; Huang, X.; Tian, F.; Li, D.; Yu, H.; Liu, Y.; Ma, Y.; Liu, B.; Cui, T. *Phys. Rev. B: Condens. Matter Mater. Phys.* **2015**, *91*, 180502.
(16) Errea, I.; Calandra, M.; Pickard, C. J.; Nelson, J.; Needs, R. J.; Li, Y.; Liu, H.; Zhang, Y.; Ma, Y.; Mauri, F. *Phys. Rev. Lett.* **2015**, *114*, 157004.
(17) Akashi, R.; Kawamura, M.; Tsuneyuki, S.; Nomura, Y.; Arita, R. *Phys. Rev. B: Condens. Matter Mater. Phys.* **2015**, *91*, 224513.
(18) Zhong, X., Wang, H., Zhang, J., Liu, H., Zhang, S., Song, H., Yang, G., Zhang, L., Ma, Y. *arXiv:1503.00396*.
(19) Li, Y.; Wang, L.; Liu, H.; Zhang, Y.; Hao, J.; Pickard, C. J.; Nelson, J. R.; Needs, R. J.; Li, W.; Huang, Y.; Errea, I.; Calandra, M.; Mauri, F.; Ma, Y. *Phys. Rev. B: Condens. Matter Mater. Phys.* **2016**, *93*, 020103.
(20) Zhang, S.; Wang, Y.; Zhang, J.; Liu, H.; Zhong, X.; Song, H.; Yang, G.; Zhang, L.; Ma, Y. *Sci. Rep.* **2015**, *5*, 15433.
(21) Ashcroft, N. W. *Phys. Rev. Lett.* **2004**, *92*, 187002.
(22) Drozdov, A. P., Eremets, M. I., Troyan, I. A. *arXiv:1508.06224*.
(23) Flores-Livas, J. A.; Amsler, M.; Heil, C.; Sanna, A.; Boeri, L.; Profeta, G.; Wolverton, C.; Goedecker, S.; Gross, E. K. U. *Phys. Rev. B: Condens. Matter Mater. Phys.* **2016**, *93*, 020508.
(24) Fu, Y., Du, X., Zhang, L., Peng, F., Zhang, M., Pickard, C., Needs, R. J., Singh, D. J., Zheng, W., Ma, Y. *arXiv:1510.04415*.
(25) Liu, H.; Li, Y.; Gao, G.; Tse, J. S.; Naumov, I. I. *J. Phys. Chem. C* **2016**, 10.1021/acs.jpcc.5b12009.
(26) Lonie, D. C.; Zurek, E. *Comput. Phys. Commun.* **2011**, *182*, 372−387.
(27) Lonie, D. C.; Zurek, E. *Comput. Phys. Commun.* **2011**, *182*, 2305−2306.
(28) Baettig, P.; Zurek, E. *Phys. Rev. Lett.* **2011**, *106*, 237002.
(29) Hooper, J.; Zurek, E. *Chem. - Eur. J.* **2012**, *18*, 5013−5021.
(30) Hooper, J.; Zurek, E. *ChemPlusChem* **2012**, *77*, 969−972.
(31) Shamp, A.; Hooper, J.; Zurek, E. *Inorg. Chem.* **2012**, *51*, 9333−9342.
(32) Hooper, J.; Terpstra, T.; Shamp, A.; Zurek, E. *J. Phys. Chem. C* **2014**, *118*, 6433−6447.
(33) Lonie, D. C.; Zurek, E. *Comput. Phys. Commun.* **2012**, *183*, 690.
(34) Kresse, G.; Hafner, J. *Phys. Rev. B: Condens. Matter Mater. Phys.* **1993**, *47*, 558.
(35) Perdew, J. P.; Burke, K.; Ernzerhof, M. *Phys. Rev. Lett.* **1996**, *77*, 3865.

DOI: 10.1021/jacs.5b10180
J. Am. Chem. Soc. 2016, 138, 1884−1892

(36) Blöchl, P. *Phys. Rev. B: Condens. Matter Mater. Phys.* **1994**, *50*, 17953.
(37) Gohr, S.; Grimme, S.; Söhnel, T.; Paulus, B.; Schwerdtfeger, P. *J. Chem. Phys.* **2013**, *139*, 174501.
(38) Sheppard, D.; Xiao, P.; Chemelewski, W.; Johnson, D. D.; Henkelman, G. *J. Chem. Phys.* **2012**, *136*, 074103.
(39) Giannozzi, P.; Baroni, S.; Bonini, N.; Calandra, M.; Car, R.; Cavazzoni, C.; Ceresoli, D.; Chiarotti, G. L.; Cococcioni, M.; Dabo, I.; Dal Corso, A.; de Gironcoli, S.; Fabris, S.; Fratesi, G.; Gebauer, R.; Gerstmann, U.; Gougoussis, C.; Kokalj, A.; Lazzeri, M.; Martin-Samos, L.; Marzari, N.; Mauri, F.; Mazzarello, R.; Paolini, S.; Pasquarello, A.; Paulatto, L.; Sbraccia, C.; Scandolo, S.; Sclauzero, G.; Seitsonen, A. P.; Smogunov, A.; Umari, P.; Wentzcovitch, R. M. *J. Phys.: Condens. Matter* **2009**, *21*, 395502.
(40) Allen, P. B.; Dynes, R. C. *Phys. Rev. B* **1975**, *12*, 905.
(41) Pickard, C. J.; Needs, R. J. *Nat. Phys.* **2007**, *3*, 473−476.
(42) Pickard, C. J.; Martinez-Canales, M.; Needs, R. J. *Phys. Rev. B: Condens. Matter Mater. Phys.* **2012**, *85*, 214114.
(43) Kikegawa, T.; Iwasaki, H. *Acta Crystallogr., Sect. B: Struct. Sci.* **1983**, *B39*, 158−164.
(44) Clark, S. M.; Zaug, J. M. *Phys. Rev. B: Condens. Matter Mater. Phys.* **2010**, *82*, 134111.
(45) Akahama, Y.; Kobayashi, M.; Kawamura, H. *Phys. Rev. B: Condens. Matter Mater. Phys.* **1999**, *59*, 8520.
(46) Akahama, Y.; Kawamura, H.; Carlson, S.; Le Bihan, T.; Häusermann, D. *Phys. Rev. B: Condens. Matter Mater. Phys.* **2000**, *61*, 3139.
(47) Jamieson, J. C. *Science* **1963**, *139*, 1291−1292.
(48) Seo, D.; Hoffmann, R. *J. Solid State Chem.* **1999**, *147*, 26−37.
(49) Boulfelfel, S. E.; Seifert, G.; Grin, Y.; Leoni, S. *Phys. Rev. B: Condens. Matter Mater. Phys.* **2012**, *85*, 014110.
(50) Ehlers, F. J. H.; Christensen, N. E. *Phys. Rev. B: Condens. Matter Mater. Phys.* **2004**, *69*, 214112.
(51) Häusserman, U. *Chem. - Eur. J.* **2003**, *9*, 1471−1478.
(52) Kaye, G. W. C.; Laby, T. H. *Tables of Physical and Chemical Constants*, 1995; http://www.kayelaby.npl.co.uk/.
(53) Weast, R. C.; Selby, S. M. *Handbook of Chemistry and Physics*, 1966; CRC Press/Taylor and Francis: Boca Raton, FL.
(54) Hooper, J.; Altintas, B.; Shamp, A.; Zurek, E. *J. Phys. Chem. C* **2013**, *117*, 2982−2992.
(55) Karuzawa, M.; Ishizuka, M.; Endo, S. *J. Phys.: Condens. Matter* **2002**, *14*, 10759−10762.
(56) Chan, K. T.; Malone, B. D.; Cohen, M. L. *Phys. Rev. B: Condens. Matter Mater. Phys.* **2013**, *88*, 064517.
(57) Richardson, C. F.; Ashcroft, N. W. *Phys. Rev. Lett.* **1997**, *78*, 118.
(58) McMahon, J. M.; Ceperley, D. M. *Phys. Rev. B: Condens. Matter Mater. Phys.* **2011**, *84*, 144515.
(59) Flores-Livas, J. A.; Amsler, M.; Lenosky, T. J.; Lehtovaara, L.; Botti, S.; Marques, M. A. L.; Goedecker, S. *Phys. Rev. Lett.* **2012**, *108*, 117004.
(60) Gao, G.; Oganov, A. R.; Bergara, A.; Martinez-Canales, M.; Cui, T.; Iitaka, T.; Ma, Y.; Zou, G. *Phys. Rev. Lett.* **2008**, *101*, 107002.
(61) Tse, J. S.; Yao, Y.; Tanaka, K. *Phys. Rev. Lett.* **2007**, *98*, 117004.
(62) Wang, H.; Tse, J. S.; Tanaka, K.; Iitaka, T.; Ma, Y. *Proc. Natl. Acad. Sci. U. S. A.* **2012**, *109*, 6463−6466.
(63) Pépin, C.; Loubeyre, P.; Occelli, F.; Dumas, P. *Proc. Natl. Acad. Sci. U. S. A.* **2015**, *112*, 7673−7676.
(64) Zurek, E.; Hoffmann, R.; Ashcroft, N. W.; Oganov, A. R.; Lyakhov, A. O. *Proc. Natl. Acad. Sci. U. S. A.* **2009**, *106*, 17640−17643.

NOTE ADDED IN PROOF

While revising this paper we became aware of three recent studies that used structure prediction methods coupled with DFT calculations to examine the stability of PH_n phases under pressure.[23−25] All of these studies found that none of the hydrides of phosphorus are stable with respect to the elemental phases above 100 GPa, in agreement with our work. In addition, Flores-Livas and co-workers have calculated the T_c of phases with $n = 1−3$ and one of the phases they identified was a PH_2 structure with $I4/mmm$ symmetry.

DOI: 10.1021/jacs.5b10180
J. Am. Chem. Soc. 2016, 138, 1884−1892